Membrane buckling and the determination of Gaussian curvature modulus

Mei-Ting Wang, Rui Ma,* and Chen-Xu Wu†

Fujian Provincial Key Laboratory for Soft Functional Materials Research, Research Institute for Biomimetics and Soft Matter, Department of Physics, College of Physical Science and Technology, Xiamen University, Xiamen 361005, People's Republic of China

(Received 22 February 2023; revised 7 June 2023; accepted 25 August 2023; published 19 September 2023)

Biological membranes can exhibit various morphology due to the fluidity of the lipid molecules within the monolayers. The shape transformation of membranes has been well described by the classical Helfrich theory, which consists only a few phenomenological parameters, including the mean and the Gaussian curvature modulus. Though various methods have been proposed to measure the mean curvature modulus, determining the Gaussian curvature modulus remains difficult both in experiments and in simulations. In this paper we study the buckling process of a rectangular membrane and a circular membrane subject to compressive stresses and under different boundary conditions. We find that the buckling of a rectangular membrane takes place continuously, while the buckling of a circular membrane can be discontinuous depending on the boundary conditions. Furthermore, our results show that the stress-strain relationship of a buckled circular membrane can be used to determine the Gaussian curvature modulus effectively.

DOI: 10.1103/PhysRevE.108.034802

I. INTRODUCTION

Buckling, a common phenomenon observed in our daily life [1–12], refers to the sudden change in the shape of an elastic object under compressive loads. The research of buckling can be dated back to as early as 1691, when Jacob Bernoulli studied the buckling of an elastic beam [13]. In the 18th century, Leonhard Euler and Daniel Bernoulli further developed the elastic beam theory which nowadays constitutes an important branch of continuum mechanics, and has broad applications in structural and mechanical engineering [14].

In recent years, buckling in fluid membranes has drawn the attention of many physicists [15–24]. The major components of a fluid membrane are lipid molecules, which are typically composed of a hydrophilic polar head and two hydrophobic hydrocarbon tails. In an aqueous solution, such lipid molecules assemble into a double-layer structure with the hydrophobic tails embedded inside so as to avoid water and the hydrophilic heads are exposed to the water outside, which is referred to as a lipid bilayer [25]. The lipid molecules can freely move laterally within the monolayer, a specific feature of fluid membranes different from solid shells. Therefore the buckling of a lipid membrane exhibits novel behaviors compared with that of an elastic shell, such as the anisotropic tension and negative compressibility [15,16].

The thickness ($\sim$4 nm) of a typical fluid membrane is negligible compared with its lateral dimension. When considering the deformation of the membrane on length scales that are even moderately larger than the thickness, the Helfrich theory [26,27], which treats the membrane as a continuum two-dimensional (2D) surface, has been extremely successful in many applications [28–34]. The theory only has a couple of phenomenological parameters characterizing the membrane's property, such as the mean and the Gaussian curvature modulus κ and $\bar{\kappa}$, and the spontaneous curvature c_0. The local deformation of a membrane directly depends on the mean curvature modulus κ, which makes the measurement of κ a relatively easy assay. In experiments, κ is typically obtained via the fluctuation spectrum of a planar membrane [35–37], or the force spectrum to pull a membrane tether from a spherical shape [38,39]. However, measuring the Gaussian curvature modulus $\bar{\kappa}$ is difficult because for a patch of membrane with a boundary, only deformations that alter the topology or the boundary of the patch contain information about the Gaussian curvature modulus due to the Gauss-Bonnet theorem [40,41]. For this very reason, in cellular processes which change the topology of the membrane, such as cell division, endocytosis, and exocytosis, the role of the Gaussian curvature modulus $\bar{\kappa}$ cannot be simply ignored [42–44].

Boundary conditions (BCs) are important to determine the shape of an elastic object. For a fluid membrane patch with an open edge, the Gaussian curvature modulus $\bar{\kappa}$ has a contribution to the boundary stress. This dependence has been used by molecular dynamics (MD) simulations to estimate the Gaussian curvature modulus $\bar{\kappa}$ either via the closure of a spherical vesicle [45,46] or via the edge fluctuations of a planar membrane [47]. However, both methods require the simulation of a large membrane either for a long time or with multiple repeats, and therefore are computationally expensive.

Recently, the buckling of a planar membrane has been suggested as a MD protocol to measure the mean curvature modulus κ of the membrane [16]. This buckling protocol is easy to implement, and has been proved to be robust against the coarse graining level of the lipid models and the treatment of the solvent when estimating κ [16]. Inspired by the work, in this paper, we consider two kinds of geometries

*ruima@xmu.edu.cn
†cxwu@xmu.edu.cn

of membrane, i.e., a rectangular membrane and a circular one, and respectively investigate their buckling phenomena under a compressive stress via the Helfrich theory [26,27]. Our numerical results of the stress-strain relationship for the rectangular membrane agree well with the theoretical predictions reported in the literature [16]. Moreover, through investigating the circular membrane, we find that the buckling process shows qualitatively different behaviors under distinct BCs. The stress-strain relationship under the free-hinge BC strongly depends on the Gaussian curvature modulus $\bar{\kappa}$, which therefore provides an effective method to determine the Gaussian bending rigidity of a fluid membrane through a buckling protocol.

II. THEORETICAL MODEL

We model the rectangular and the circular membranes as one-dimensional and axis-symmetric two-dimensional patches, respectively. We consider two types of BCs, namely the free-hinge BC in which the membrane is allowed to rotate freely at the edge where compressible stresses are applied, and the fixed-hinge BC in which the membrane angle is fixed to be in parallel with the substrate at the edge.

A. The rectangular membrane

For the rectangular membrane which is initially laid in a plane at the horizontal surface with a length of L_0 in the x direction and a width of L_y in the y direction, the buckling is driven by a compressive stress f_x applied at the two ends of the membrane along the x direction. When the stress f_x exceeds a critical value, the membrane will buckle with its shape depicted by the coordinates $[X(s), Z(s)]$, where s is the arc length along the x direction (Fig. 1). We assume that the total arc length L_0 of the membrane is invariant during the buckling process and introduce $\psi(s)$ as the angle made between the tangential direction of the arc and the x direction. The total energy of the membrane is written as

$$E = \frac{\kappa}{2}\int c_1^2 dA + f_x L_x L_y, \tag{1}$$

where the first term is the bending energy, with $c_1 = d\psi/ds$ the principal curvature along the arc direction, and $dA = L_y ds$ the area element. The second term is the boundary energy, where the compressive stress f_x is essentially a Lagrangian multiplier with a unit of force per unit length imposed on the base length L_x in the x direction. Note that the Gaussian curvature for the curved rectangular membrane is zero, and therefore has no contribution to the total energy.

B. The circular membrane

For the circular membrane which is initially laid in a plane with a radius of R_0, the buckling is driven by a compressive stress f_r along the inward radial direction applied at the perimeter of the membrane. When the stress exceeds a critical value, the membrane will buckle with the shape of the membrane depicted by the coordinates $[R(s), Z(s)]$, where s is the arc length along the meridian direction, as shown in Fig. 2. Different from the rectangular membrane, the total arc length S can change during buckling, but the total area A of

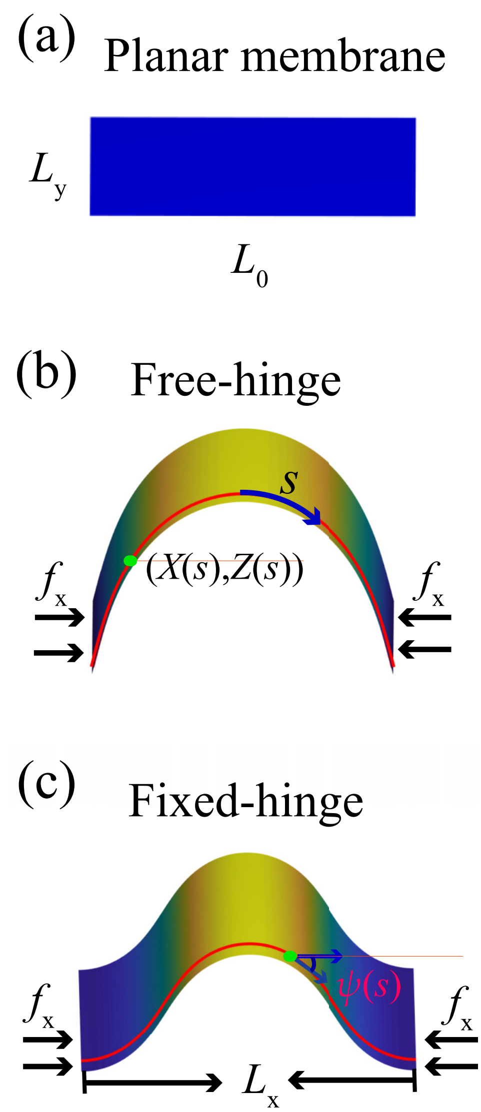

FIG. 1. Illustration of a rectangular membrane deformed from (a) a planar shape, to a buckled shape under (b) free-hinge BC or (c) fixed-hinge BC.

the membrane remains invariant, the same as in the rectangular membrane. The angle $\psi(s)$ spans between the tangential meridian direction and the radial direction. The total energy of the membrane reads

$$F = \int \left[\frac{\kappa}{2}(c_1 + c_2)^2 + \bar{\kappa} c_1 c_2\right] dA + \sigma A + f_r \pi R_b^2, \tag{2}$$

where we use F to denote energy for the circular membrane instead of E for the rectangular membrane. The first integral is the bending energy with $c_1 = d\psi/ds$ and $c_2 = \sin\psi/R$ the two principal curvatures of the membrane surface, and the two terms in the square brackets represent contributions from the mean curvature and the Gaussian curvature, respectively. The Lagrangian multiplier σ in the second term is to impose a constant surface area condition for the membrane during the buckling process, which can be interpreted as the membrane tension. The last term is the boundary energy, where the compressive stress f_r is also a Lagrangian multiplier imposed on

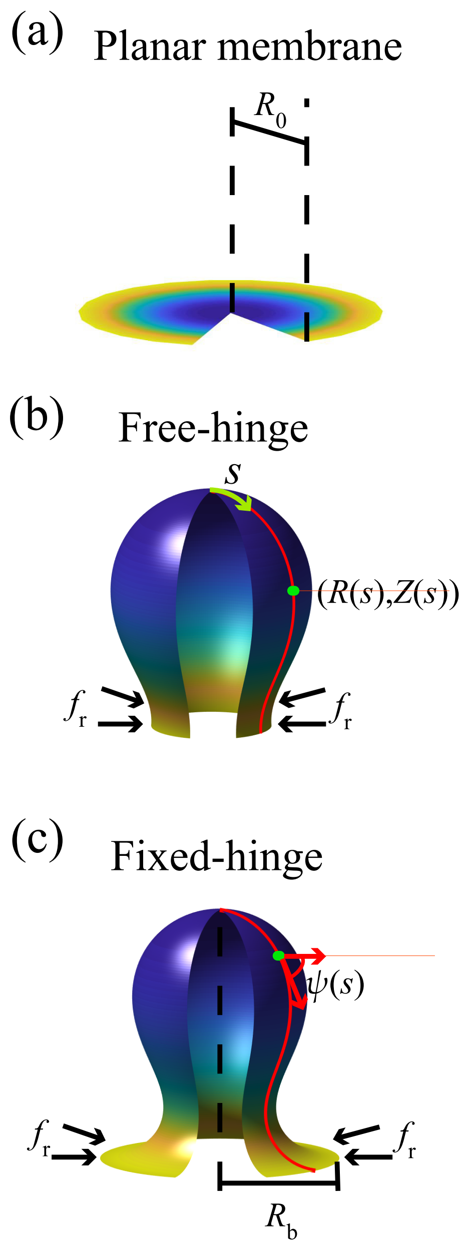

FIG. 2. Illustration of a circular membrane deformed from (a) a planar circular shape, to a buckled shape under (b) free-hinge BC or (c) fixed-hinge BC.

the base area πR_b^2 with R_b the base radius of the membrane when it buckles.

C. Boundary conditions

For the free-hinge BC, we have the vanishing bending moment at the boundary. In the case of the rectangular membrane, it is expressed as the vanishing curvature $c_1 = 0$. In the case of the circular membrane [Fig. 2(b)], it implies that

$$\kappa(c_1 + c_2) + \bar{\kappa} c_2 = 0. \tag{3}$$

Note that the Gaussian curvature modulus $\bar{\kappa}$ appears in Eq. (3). This is the key reason why we can use the buckling protocol to measure $\bar{\kappa}$ for the free-hinge BC, which will be elaborated later.

For the fixed-hinge BC, we simply fix the membrane angle $\psi = 0$ unless otherwise stated, as illustrated in Fig. 2(c) in the case of the circular membrane.

III. RESULTS AND DISCUSSION

A. The buckling of a rectangular membrane

The buckling of a rectangular membrane with a fixed-hinge BC has been studied both analytically and via MD simulations in Refs. [15,16]. Here, we numerically solve the shape equations and analyze the buckling process from an energetic point of view and incorporate the free-hinge BC into consideration. The detailed derivations of the shape equations, as well as the BCs, are presented in Appendix A. We numerically solve the shape equations via the MATLAB solver bvp5c, which is designed for boundary value problems of ordinary differential equations. A description of how to use the solver to iteratively obtain membrane shapes of different buckling degree is provided in Appendix C.

The planar shape is always a trivial solution to the shape equations regardless of the stress f_x and the BCs, and the total energy E_p of the planar shape increases with the stress f_x linearly due to the boundary energy (cyan line in Fig. 3). When the stress f_x exceeds a critical value, a new branch of solutions emerges due to membrane buckling (Fig. 3, black dotted line). The total energy of the buckled shape is lower than that of the planar shape, indicating that as the stress increases to the critical point, the rectangular membrane will experience a buckling transition, at which membrane starts to bend with an increasing bending energy E_b at the cost of reduced boundary energy E_l.

Near the critical stress, the buckled membrane remains relatively planar. As the stress builds up, the membrane becomes more and more bent (top panels in Fig. 3). In order to describe the bending degree, we define the strain $\mu_x = (L_0 - L_x)/L_0$ and plot the stress-strain relationship in Fig. 4. Buckling is featured in the nonzero value of the stress f_x at $\mu_x = 0$. We find that the stress required to bend the membrane to the same strain for the fixed hinge is fourfold of that for the free hinge. Furthermore, we compare our numerical results with the analytical results for the fixed-hinge BC derived in Ref. [16],

$$f_x = \kappa\left(\frac{2\pi}{L_0}\right)^2\left[1 + \frac{1}{2}\mu_x + \frac{9}{32}\mu_x^2 + \frac{21}{128}\mu_x^3 + O(\mu_x^4)\right], \tag{4}$$

and find good agreement between them (the red solid line and the red dashed line in Fig. 4).

B. The buckling of a circular membrane with zero Gaussian curvature modulus

In this section, we study the buckling process of a circular membrane under an isotropic and compressible radial stress f_r with a unit of force per unit length. The membrane shape is assumed to remain axisymmetric upon buckling and thus can be depicted using its meridian profile. The shape equations, as well as the BCs, for the axisymmetric circular membranes are derived in Appendix B. In order to see the differences made by $\bar{\kappa} = 0$ and $\bar{\kappa} \neq 0$, we first study the condition $\bar{\kappa} = 0$ and show the effect of nonzero $\bar{\kappa}$ in the next section. It is found that the

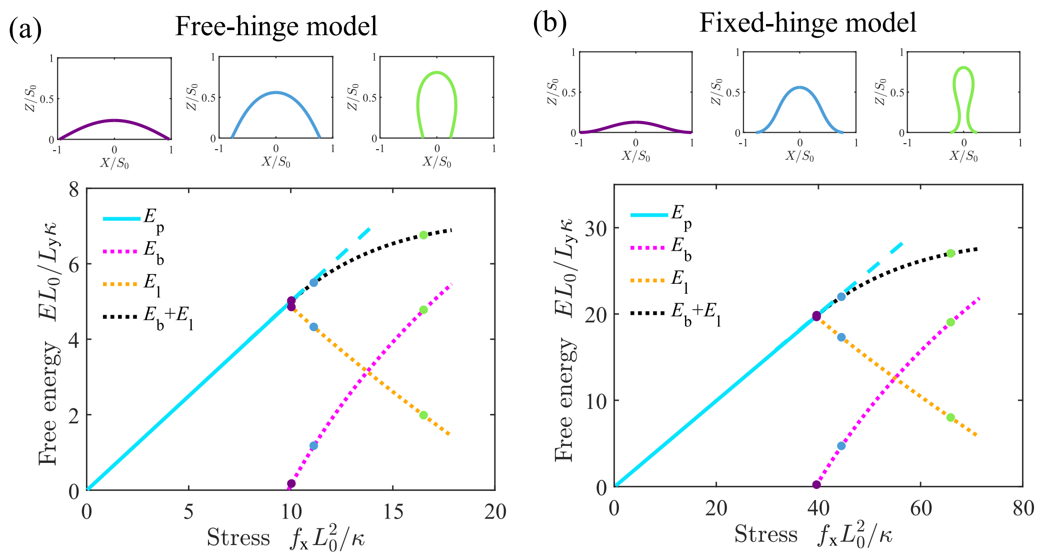

FIG. 3. Effect of the stress on the free energy of the rectangular membrane based on (a) a free-hinge or (b) a fixed-hinge model. Here, $S_0 = L_0/2$.

buckling behaviors for the two types of BCs are qualitatively different. For the sake of comparison, we introduce the area strain $\mu_r = (A_0 - A_b)/A_0$ to reflect the buckling degree of the circular membrane, with $A_0 = \pi R_0^2$ the total surface area and $A_b = \pi R_b^2$ the base area when the membrane buckles.

For the free-hinge BC, the buckling process is quite similar to that of the rectangular membrane. With the increase of the stress f_r, a new branch of buckling solution emerges in addition to the planar membrane [black dotted line and cyan line in Fig. 5(a)]. The total energy of the buckled membrane, consisting of the bending energy F_b and the boundary energy F_l, is lower than that of the planar membrane F_p, indicating the occurrence of a buckling transition. The membrane remains almost planar near the transition point, and after that the buckling degree continuously increases with the stress f_r [top panels in Fig. 5(a)], which is manifested as a continuous stress-strain relationship in the blue curve of Fig. 6. We analytically derive the critical stress (see Appendix E for the detailed derivation).

$$f_r^{\text{crit}} = \kappa \frac{\left[x_1^{(0)}\right]^2}{R_0^2}, \tag{5}$$

a result in good agreement with the numerical solution (the magenta star in Fig. 6). For the fixed-hinge BC, the energy profiles become complicated and two buckling branches are found for a single stress f_r. On one of the buckling branches, the bending degree decreases with the increasing stress f_r [the purple and the blue shapes of the top panels in Fig. 5(b)]. Hereafter, we will refer to this branch as branch 1. On the other branch, the base of the membrane is nearly closed [the green shape of the top right panel in Fig. 5(b)]. Hereafter, we will refer to this branch as branch 2. The total energy, consisting of the bending energy F_b and the boundary energy F_l, is lower in branch 2 than in branch 1. The energy of the planar membrane intersects with branch 2 at a point such that the membrane is nearly closed. All these results suggest that for the fixed-hinge BC, there exists a first-order transition at the critical stress, beyond which a sudden and sharp membrane buckling occurs. In the stress-strain relationship, it is reflected in the sudden jump of the strain from zero to almost 1 when the stress goes beyond the critical point (the red curve in Fig. 6). To further understand the origin of the first-order transition under the fixed-hinge BC, we calculate the buckling process of a circular membrane under different hinged angles. Note that for a nonzero hinged angle, the membrane is already bent even at zero stress f_r. It is found that if the hinged angle is large, the total energy of the buckled membrane continuously increases with f_r (the orange line in Fig. 7). However, for small hinged angles, a Gibbs triangle appears in the energy profile (the magenta, the black, and the green lines in Fig. 7), which is the characteristic of a first-order transition. A further calculation tells us that the critical angle distinguishing between the first-order and the second-order transitions is around 0.257π, as indicated by the red dotted line in Fig. 7.

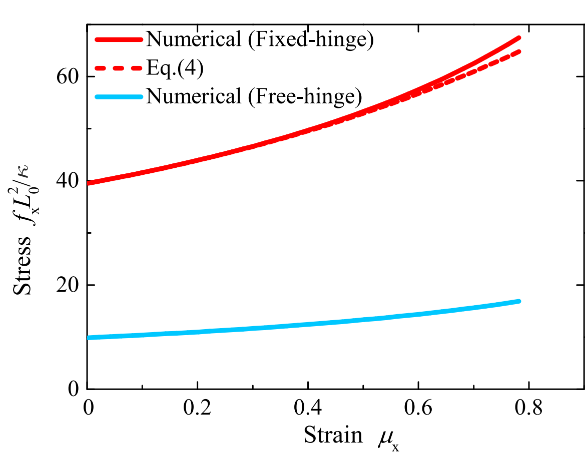

FIG. 4. Stress-strain relationship of the rectangular membrane. The dashed red curve represents the analytical result Eq. (4) reported in Ref. [16].

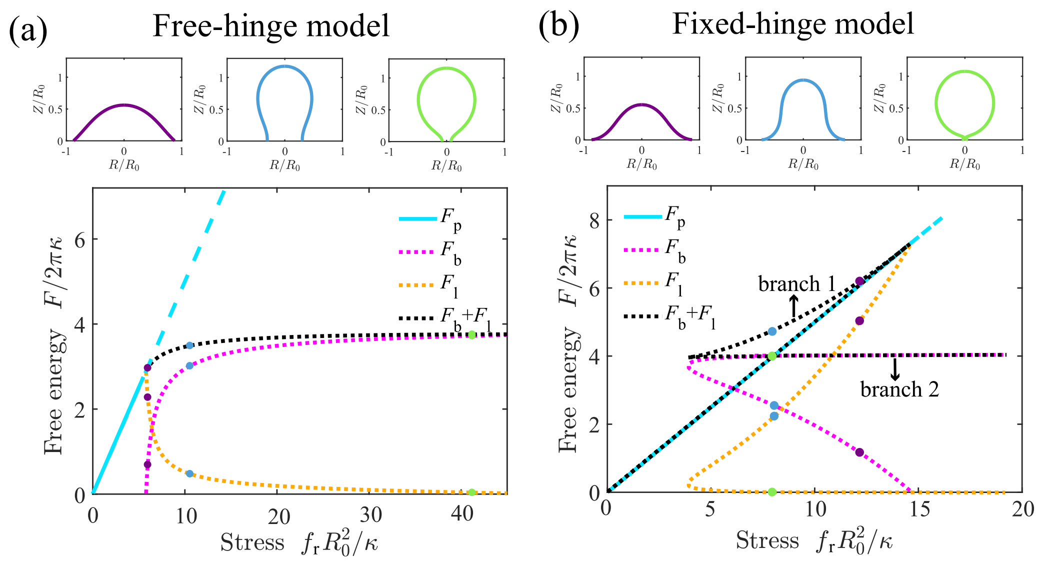

FIG. 5. Dependence of the total energy of the circular membrane with Gaussian curvature modulus $\bar{\kappa}/\kappa = 0$ on the stress based on (a) free-hinge BC and (b) fixed-hinge BC, respectively.

C. Determination of the Gaussian curvature modulus via circular membrane buckling with a free-hinge BC

In this section, we study the effect of the Gaussian curvature modulus $\bar{\kappa}$ on the buckling process of a circular membrane under the free-hinge BC condition Eq. (3), in which $\bar{\kappa}$ explicitly appears. By virtue of the fact that the Gaussian curvature modulus $\bar{\kappa}$ only contributes to the boundary bending moment, it makes no difference on the membrane shape equations, and therefore has no impact on the buckling process under the fixed-hinge BC in which $\psi = 0$ has no dependence on $\bar{\kappa}$.

In Fig. 8, we show the total energy $F = F_b + F_l$ of a buckled membrane as a function of the stress f_r with different Gaussian curvature moduli under the free-hinge BC. It is found that the energy of the planar membrane intersects with the energy of the buckled membrane at two stresses [cyan lines in Figs. 8(a)–8(c)]. After crossing the smaller stress point, the energy of the planar membrane remains lower than that of the buckled one until it reaches the larger stress point, indicating that the buckling actually occurs at the larger stress point. Furthermore, the strain at the buckling point is nonzero, which implies a discontinuous transition. It is found that the critical stress f_r^{crit} and its corresponding strain μ_r^{crit} both increase with the absolute value of the Gaussian curvature modulus $|\bar{\kappa}/\kappa|$, as shown in Fig. 8(d).

In principle, the Gaussian bending modulus can be determined from Fig. 8(d) if we can measure the critical buckling stress f_r^{crit} and the corresponding critical strain μ_r^{crit} for a circular membrane under the free-hinge BC from MD simulations. However, the precision of the measurement will be limited by the single variable measurement. To overcome this issue, we find out that the stress-strain relationships for different Gaussian curvature moduli are quite different, as shown in Fig. 9. Calibrating the stress-strain curves with this figure provides a more robust way to estimate the Gaussian curvature modulus $\bar{\kappa}$. To elaborate the idea, we consider a typical MD simulation of a membrane patch with 1000 lipid

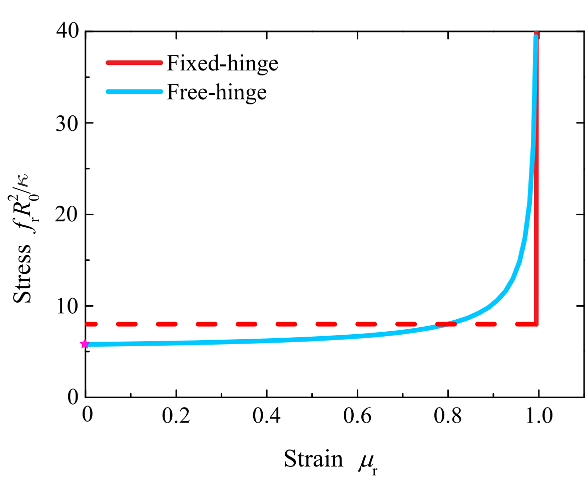

FIG. 6. Stress-strain relationship of the buckled circular membrane with $\bar{\kappa}/\kappa = 0$. The magenta star indicates the analytical result for the critical buckling stress given by Eq. (5).

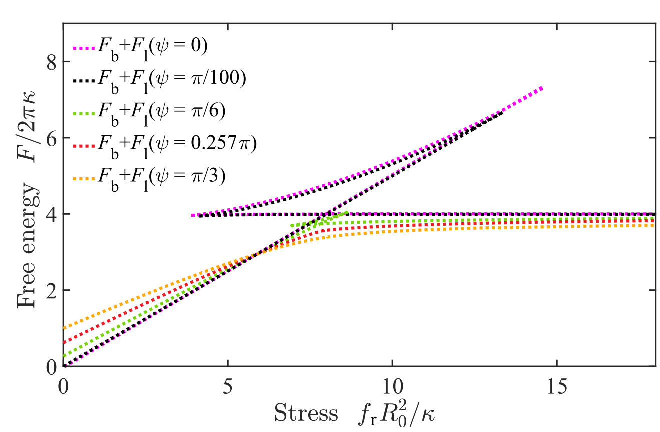

FIG. 7. Effect of the stress on the total energy of the circular membrane under the fixed-hinge BC for different hinged angles.

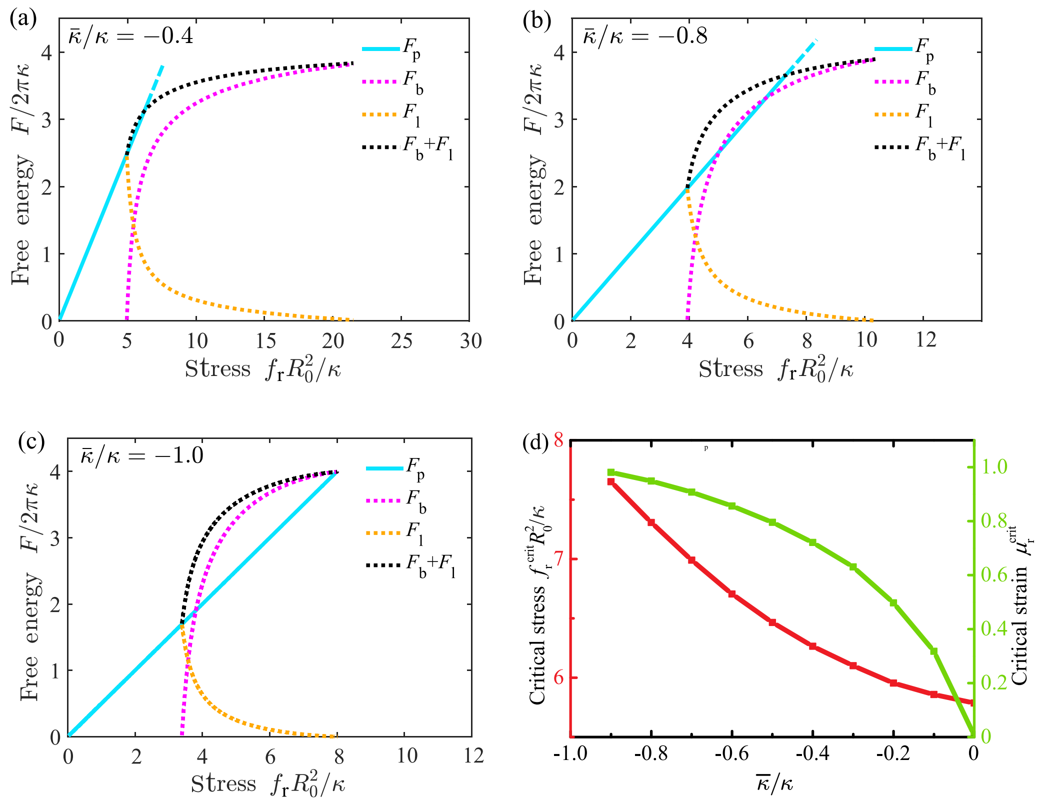

FIG. 8. Dependence of the free energy of the circular membrane on the stress under the free-hinge condition with three different Gaussian curvatures (a) $\bar{\kappa}/\kappa = -0.4$, (b) $\bar{\kappa}/\kappa = -0.8$, and (c) $\bar{\kappa}/\kappa = -1.0$. (d) The critical stress $f_{\rm r}^{\rm crit}$ (red curve) and its corresponding strain $\mu_{\rm r}^{\rm crit}$ (green curve) as a function of Gaussian curvature $\bar{\kappa}/\kappa$ under the free-hinge condition, respectively.

molecules [48–51]. Assuming each lipid occupies an area of 0.5 nm^2 [52], the total surface area of the patch is 500 nm^2 and the radius of the circular membrane $R_0 = 12.6$ nm. Assuming that the mean curvature modulus κ is known, e.g., $\kappa = 40\,k_{\rm B}T$, from the rectangular membrane buckling simulations, our aim is to determine the ratio of $\bar{\kappa}/\kappa$ as accurately

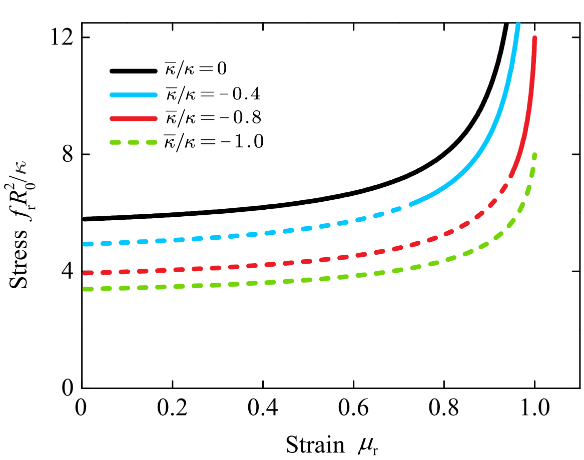

FIG. 9. The stress-strain relationship of the circular membrane with different Gaussian curvature moduli. The solid part represents the stress-strain relation beyond the critical stress such that the buckled shape is stable, and the dashed part represents the stress-strain relation below the critical stress, where the buckled shape is metastable and the planar shape is stable.

as possible from the stress-strain relationship of the buckled circular membrane. The stress applied at the boundary of the patch can be precisely regulated in a MD simulation by tuning the forces acting on the lipid molecules at the boundary. However, the strain, i.e., the base radius of the membrane patch $R_{\rm b}$, needs to be read out from the simulation and it has an uncertainty due to thermal fluctuations. In Fig. 10, we show the calculated base radius $R_{\rm b}$ as a function of the ratio $\bar{\kappa}/\kappa$ at three different stresses. Imagine in a hypothetical simulation, the stress is tuned at $f_{\rm r} = 6.9$ pN/nm and the circular membrane is buckled and compressed to a base radius of $R_{\rm b} = 6 \pm 1$ nm. We can then read out the ratio $\bar{\kappa}/\kappa = -0.38$, and the confidence interval is $[-0.56, -0.17]$, as illustrated in Fig. 10. Note that when the stress is small, buckling only occurs for small values of $|\bar{\kappa}/\kappa|$, as shown by the solid part of the green curve ($f_{\rm r} = 6.3$ pN/nm) in Fig. 10. In order to improve the accuracy, we can measure the base radius at multiple stresses and the confidence interval would be the joint set of each readout. For instance, raising the stress up to 7.9 pN/nm would give another measurement of the base radius, from which the average value and the confidence interval of $\bar{\kappa}/\kappa$ can be read out from the red curve in Fig. 10. Compared with measuring the fluctuation spectrum at the edge, obtaining the stress-strain relationship is more straightforward. We speculate the method is also robust against the coarse graining level of the lipid models and the treatment of the solvent based on its performance in the measurement of the mean curvature modulus κ [16]. A test of the method with MD simulations will be included in one of our future works.

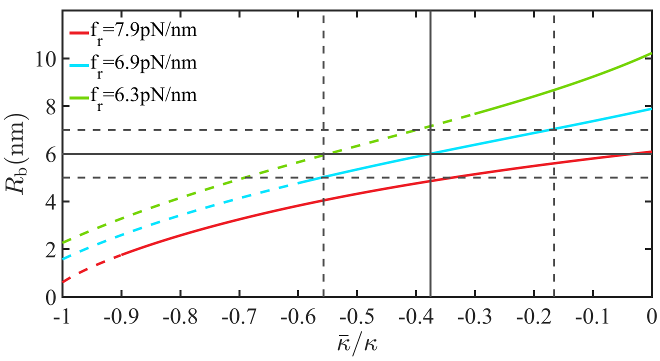

FIG. 10. The base radius as a function of the ratio $\bar{\kappa}/\kappa$ at different stresses for a hypothetical MD simulation. The membrane patch is assumed to have a surface area of 500 nm^2 and has a mean curvature modulus of $\kappa = 40k_BT$. For each curve, the solid/dashed part represents the region where the applied stress is greater/less than the critical buckling stress, respectively. The horizontal solid line indicates the measured value of $R_b = 6$ nm in a hypothetical simulation and the two horizontal dashed lines indicate the uncertainty of the measurement. The vertical solid line indicates the predicted value of the ratio $\bar{\kappa}/\kappa = -0.38$ and the vertical dashed lines indicate the confidence interval of the prediction.

IV. DISCUSSION AND CONCLUSION

One of the aims of this paper is to investigate the role of the Gaussian curvature modulus $\bar{\kappa}$ in the buckling process of a membrane. It is best manifested in the buckling process of a circular membrane under free-hinge BC, which exhibits a continuous transition for zero $\bar{\kappa}$ (shown in Sec. III B), but a discontinuous transition for nonzero $\bar{\kappa}$ (shown in Sec. III C). Furthermore, the stress-strain curves for membranes with different nonzero Gaussian curvature moduli $\bar{\kappa}$ differ in two aspects: (i) The critical stress and the corresponding critical strain are different. A more negative $\bar{\kappa}$ leads to a larger critical stress $f_r^{\rm crit}$ and critical strain $\mu_r^{\rm crit}$ [Fig. 8(d)]. (ii) Beyond the critical stress, the stress-strain curves are also quantitatively different (Fig. 9). The differences can be exploited to accurately quantify the Gaussian curvature moduli $\bar{\kappa}$. A possible drawback of the method is that when the Gaussian curvature modulus is very negative ($\bar{\kappa}/\kappa \approx -1$), the base radius R_b can be very small when buckling takes place. For instance, the buckled base radius $R_b < 2$ nm if $\bar{\kappa}/\kappa = -0.9$ in the hypothetical simulation, as illustrated in the red curve of Fig. 10. In this case, the MD simulation of buckling might be difficult to achieve as the membrane is almost in closure at the base.

In summary, we investigate, respectively, the buckling of a rectangular membrane and a circular membrane under two BCs. It is found that for an initially planar rectangular membrane, when the stress from two sides is increasingly loaded, buckling occurs continuously under both free-hinge and fixed-hinge BCs. But for the initially planar circular membrane, the buckling behavior depends on its boundary condition, as well as the Gaussian curvature moduli. For the fixed-hinge BC, there exists a first-order buckling transition if the hinged angle is small, regardless of the Gaussian curvature modulus $\bar{\kappa}$. For the free-hinge BC, with the increase of stress, buckling takes place continuously for zero $\bar{\kappa}$ and discontinuously for nonzero $\bar{\kappa}$. Finally, we find an effective method to determine the Gaussian curvature modulus by calibrating the stress-strain relationship of the circular membrane under the free-hinge BC with different Gaussian curvature moduli.

ACKNOWLEDGMENTS

We acknowledge financial support from National Natural Science Foundation of China under Grants No. 12147142, No. 11974292, No. 12174323, and No. 12004317, Fundamental Research Funds for Central Universities of China under Grant No. 20720200072 (R.M.), and 111 Project No. B16029.

APPENDIX A: SHAPE EQUATIONS AND BOUNDARY CONDITIONS FOR RECTANGULAR MEMBRANES

For the rectangular membrane, one can obtain its principal curvature $c_1 = \dot{\psi}$. The elastic energy E in Eq. (1) then can be written as $E = \kappa L_y \int_0^{L_0/2} \mathcal{L} ds$, with its Lagrangian function given by

$$\mathcal{L} = \frac{1}{2}\dot{\psi}^2 + \bar{f}_x \cos\psi + \gamma(\dot{X} - \cos\psi) + \eta(\dot{Z} + \sin\psi), \tag{A1}$$

where $\bar{f}_x = f_x/\kappa$, $\dot{\psi}$ and $\dot{X}$ denote their derivatives with respect to the arc length s, and γ and η are the Lagrangian multipliers that enforce the geometric relations

$$\dot{X} = \cos\psi, \quad \dot{Z} = -\sin\psi. \tag{A2}$$

A variation of the functional E gives

$$\begin{aligned}\frac{\delta E}{\kappa L_y} = &\int_0^{L_0/2} ds\left\{\left[\frac{\partial\mathcal{L}}{\partial\psi} - \frac{d}{ds}\frac{\partial\mathcal{L}}{\partial\dot{\psi}}\right]\delta\psi + \left[\frac{\partial\mathcal{L}}{\partial X} - \frac{d}{ds}\frac{\partial\mathcal{L}}{\partial\dot{X}}\right]\delta X \right.\\ &\left. + \left[\frac{\partial\mathcal{L}}{\partial Z} - \frac{d}{ds}\frac{\partial\mathcal{L}}{\partial\dot{Z}}\right]\delta Z + \frac{\partial\mathcal{L}}{\partial\gamma}\delta\gamma + \frac{\partial\mathcal{L}}{\partial\eta}\delta\eta\right\}\\ &- H\delta s\Big|_0^{L_0/2} + \frac{\partial\mathcal{L}}{\partial\dot{\psi}}\delta\psi\Big|_0^{L_0/2} + \frac{\partial\mathcal{L}}{\partial\dot{X}}\delta X\Big|_0^{L_0/2} + \frac{\partial\mathcal{L}}{\partial\dot{Z}}\delta Z\Big|_0^{L_0/2},\end{aligned} \tag{A3}$$

where $H \equiv -\mathcal{L} + \dot{\psi}\partial\mathcal{L}/\partial\dot{\psi} + \dot{X}\partial\mathcal{L}/\partial\dot{X} + \dot{Z}\partial\mathcal{L}/\partial\dot{Z}$ is the Hamiltonian function given by

$$H = \frac{1}{2}\dot{\psi}^2 - \bar{f}_x\cos\psi + \gamma\cos\psi - \eta\sin\psi. \tag{A4}$$

Having the bulk terms of Eq. (A3) vanish leads to the shape equations

$$\ddot{\psi} = \dot{\psi} + \gamma\sin\psi + \eta\cos\psi - \bar{f}_x\sin\psi, \tag{A5}$$

$$\dot{\gamma} = 0, \tag{A6}$$

$$\dot{\eta} = 0. \tag{A7}$$

Having the boundary terms in Eq. (A3) vanish, one can obtain the BCs. In particular, at the membrane tip where $s = 0$, we have four BCs: $\psi(0) = 0$, $X(0) = 0$, $\gamma(0) = \bar{f}_x - [\dot{\psi}(0)]^2/2$, and $\eta(0) = 0$. At the membrane base where $s = L_0/2$, we have three BCs: $Z(L_0/2) = 0$, $X(L_0/2) = L_x/2$, and $\psi(L_0/2) = 0$ for the fixed-hinge BC or $\dot{\psi}(L_0/2) = 0$ for the free-hinge BC.

In summary, Eqs. (A2) and (A5)–(A7) constitute the full set of shape equations for rectangular membranes. They can be converted to six first-order ordinary differential equations.

Together with the unknown Lagrangian multiplier $\bar{f}_{\mathrm{x}}$ and the seven BCs, we solve the problem with the bvp5c solver in MATLAB that is designed for solving the boundary value problems of ordinary differential equations.

APPENDIX B: SHAPE EQUATIONS AND BOUNDARY CONDITIONS FOR CIRCULAR MEMBRANES

For the circular membrane, the meridian coordinates $R(s)$ and $Z(s)$ satisfy the geometric relations via

$$\dot{R} = \cos\psi, \quad \dot{Z} = -\sin\psi. \tag{B1}$$

The elastic energy F in Eq. (2) can be expressed as $F = 2\pi\kappa\int_0^S \mathcal{L}ds$, with its Lagrangian function given by

$$\mathcal{L} = \frac{R}{2}\left(\dot{\psi} + \frac{\sin\psi}{R}\right)^2 + \bar{\kappa}\dot{\psi}(\sin\psi)/\kappa + \bar{\sigma}R + \bar{f}_{\mathrm{r}}R\cos\psi$$
$$+\gamma(\dot{R} - \cos\psi) + \eta(\dot{Z} + \sin\psi), \tag{B2}$$

where $\bar{\sigma} = \sigma/\kappa$, $\bar{f}_{\mathrm{r}} = f_{\mathrm{r}}/\kappa$, and $\gamma(s)$ and $\eta(s)$ are Lagrangian multipliers to enforce the geometric relations in Eq. (B1). The total arc length S is an unknown parameter to be solved with shape equations. A variation of the functional F reads

$$\frac{\delta F}{2\pi\kappa} = \int_0^S ds\left\{\left[\frac{\partial\mathcal{L}}{\partial\psi} - \frac{d}{ds}\frac{\partial\mathcal{L}}{\partial\dot{\psi}}\right]\delta\psi + \left[\frac{\partial\mathcal{L}}{\partial R} - \frac{d}{ds}\frac{\partial\mathcal{L}}{\partial\dot{R}}\right]\delta R\right.$$
$$\left.+\left[\frac{\partial\mathcal{L}}{\partial Z} - \frac{d}{ds}\frac{\partial\mathcal{L}}{\partial\dot{Z}}\right]\delta Z + \frac{\partial\mathcal{L}}{\partial\gamma}\delta\gamma + \frac{\partial\mathcal{L}}{\partial\eta}\delta\eta\right\}$$
$$-H\delta s\Big|_0^S + \frac{\partial\mathcal{L}}{\partial\dot{\psi}}\delta\psi\Big|_0^S + \frac{\partial\mathcal{L}}{\partial\dot{R}}\delta R\Big|_0^S + \frac{\partial\mathcal{L}}{\partial\dot{Z}}\delta Z\Big|_0^S, \tag{B3}$$

where the Hamiltonian function $H \equiv -\mathcal{L} + \dot{\psi}\partial\mathcal{L}/\partial\dot{\psi} + \dot{R}\partial\mathcal{L}/\partial\dot{R} + \dot{Z}\partial\mathcal{L}/\partial\dot{Z}$ can be expressed as

$$H = \frac{R}{2}\left[\dot{\psi}^2 - \left(\frac{\sin\psi}{R}\right)^2\right] - \bar{\sigma}R - \bar{f}_{\mathrm{r}}R\cos\psi$$
$$+\gamma\cos\psi - \eta\sin\psi = 0. \tag{B4}$$

If we have the bulk terms of Eq. (B3) vanish, we obtain the following shape equations,

$$\ddot{\psi} = \frac{\sin\psi\cos\psi}{R^2} - \frac{\dot{\psi}}{R}\cos\psi + \frac{\gamma}{R}\sin\psi$$
$$+\frac{\eta}{R}\cos\psi - \bar{f}_{\mathrm{r}}\sin\psi, \tag{B5}$$

$$\dot{\gamma} = \frac{1}{2}\dot{\psi}^2 - \frac{\sin^2\psi}{2R^2} + \bar{\sigma} + \bar{f}_{\mathrm{r}}\cos\psi, \tag{B6}$$

$$\dot{\eta} = 0. \tag{B7}$$

The BCs can be obtained by setting the boundary terms in Eq. (B3) to be zero. In particular, at the membrane tip $s = 0$, we have four BCs: $\psi(0) = 0$, $R(0) = 0$, $\gamma(0) = 0$, and $\eta(0) = 0$. At the membrane base $s = S$, we have three BCs: $Z(S) = 0$, $R(S) = R_{\mathrm{b}}$, $\psi(S) = 0$ for the fixed-hinge BC or $\kappa(\dot{\psi} + \sin\psi/R) + \bar{\kappa}\sin\psi/R = 0$ for the free-hinge BC. In addition, we need to impose the incompressibility condition

$$2\pi\int_0^S r ds = \pi R_0^2. \tag{B8}$$

In summary, Eqs. (B1) and (B5)–(B7) make up the full set of shape equations for circular membranes. They can be converted to six first-order ordinary differential equations. Together with the two unknown parameter $\bar{f}_{\mathrm{r}}$ and S, as well as the seven BCs and the incomprehensibility constraint (B8), we can solve the problem with the MATLAB solver bvp5c.

APPENDIX C: DESCRIPTION OF THE NUMERICAL METHOD

We use the bvp5c solver in MATLAB to solve the boundary value problem composed by the shape equations and the BCs provided in Appendixes A and B. The bvp5c solver is based on a finite-difference method that implements the four-stage Lobatto IIIa formula [53]. When using the solver, in addition to providing the shape equations and the BCs, we also need to pass the function with an initial guess of the solution. We adopt an iterative strategy to get membrane shapes with different buckling degrees by starting with an almost planar shape. In the case of rectangular membranes, the planar shape means that $L_{\mathrm{x}} \approx L_0$ or $\mu_{\mathrm{x}} \approx 0$. In the case of circular membranes, it corresponds to a large R_{b} that is almost the maximum value limited by the surface area of the patch. Once we obtain the first solution for the large L_{x} or R_{b}, we iteratively reduce the value of L_{x} or R_{b} in small increments, and use the solution of the previous step as the initial guess for the current step. In this way, we obtain solutions of the shape equations of various strains. The stress is obtained from the unknown parameter solved by the bvp5c solver.

APPENDIX D: ACCURACY TEST OF THE NUMERICAL METHODS

In order to verify the accuracy of our numerical solutions to the membrane shape equations, we compare our numerical results with the analytical results provided in Ref. [16] for a rectangular membrane with a fixed-hinge BC. The analytical expression of the membrane shape reads

$$X(s) = 2\lambda\mathrm{E}[\mathrm{am}[s/\lambda, m], m] - s, \tag{D1a}$$

$$Z(s) = 2\lambda\sqrt{m}(1 - \mathrm{cn}[s/\lambda, m]), \tag{D1b}$$

where $\lambda = \sqrt{\kappa/f_{\mathrm{x}}}$ and $m = \sin^2(\psi_{\mathrm{i}}/2)$ [16]. Here, $s \in [0, L_0]$ is the arc length from one end to the other end, $\mathrm{am}[s/\lambda, m]$ is the amplitude of Jacobian elliptic function, $\mathrm{E}[\mathrm{am}[s/\lambda, m], m]$ is the incomplete elliptic integral of the second kind, $\mathrm{cn}[s/\lambda, m]$ is the Jacobian elliptic function, and ψ_{i} is the angle of the point on the rectangular membrane where the curvature disappears $d\psi/ds = 0$, in other words, the inflection point. We find good agreement between our numerical results and the analytical expression (the cyan solid line and the magenta dashed line as shown in Fig. 11), thus proving the accuracy of our method at least in this particular problem.

APPENDIX E: ANALYTICAL RESULTS FOR THE CRITICAL BUCKLING STRESS OF A CIRCULAR MEMBRANE UNDER THE FREE-HINGE BOUNDARY CONDITION

For an almost planar membrane, the angle $\psi \ll 1$. Under this approximation, we can get the linearized shape equation

$$R^2\psi'' + R\psi' - (R^2\bar{\sigma} + 1)\psi = 0, \tag{E1}$$

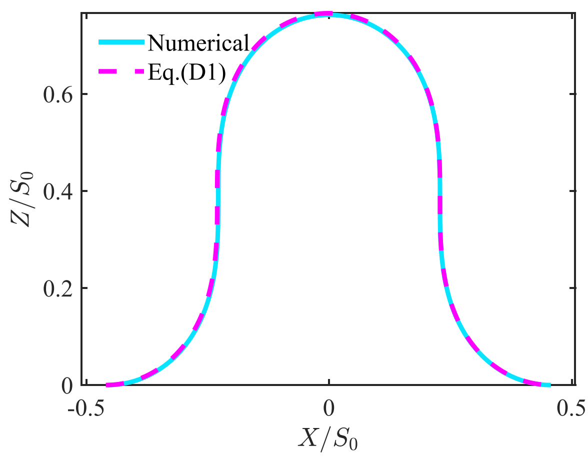

FIG. 11. Membrane shape of our numerical results (solid cyan curve) compared with the analytical results of Ref. [16] (dashed magenta curve). Here, we choose $\psi_{\rm i} = \pi/2$ and $m = \sin^2(\psi_{\rm i}/2) = 0.5$. The corresponding strain $\mu_{\rm x}$ for the numerical solution can be obtained via the expression $\mu_{\rm x} \equiv (L_0 - L_{\rm x})/L_0 = 2(1 - {\rm E}[m]/{\rm K}[m]) = 0.54$, where E[$m$] is the complete elliptic integral of the second kind, and K[m] is the complete elliptic integral of the first kind.

where we have converted the function $\psi(s)$ to $\psi(R)$ with the prime denoting the derivative with respect to R. The equation has a physically meaningful solution

$$\psi(R) = C_1 J_1(R\sqrt{-\bar{\sigma}}), \tag{E2}$$

only if $\bar{\sigma} < 0$. Here, C_1 is an arbitrary constant and $J_1(x)$ denotes the first kind of Bessel function. The free-hinge BC requires that the following equation,

$$\psi' + \frac{\psi}{R} = 0, \tag{E3}$$

holds at $R = R_{\rm b}$. Substituting Eq. (E2) into (E3), we obtain

$$J_0(R_{\rm b}\sqrt{-\bar{\sigma}}) = 0. \tag{E4}$$

In order to get the first buckling mode, we let $R_{\rm b}\sqrt{-\bar{\sigma}} = x_1^{(0)}$, the first zero value of the Bessel function $J_0(x)$. The resulting membrane tension reads

$$\bar{\sigma} = -\frac{1}{R_{\rm b}^2}\left[x_1^{(0)}\right]^2. \tag{E5}$$

The critical stress at which buckling occurs is essentially the negative tension in Eq. (E5) and has the base radius $R_{\rm b} = R_0$. In this way, we obtain Eq. (5).

[1] R. M. Jones, *Buckling of Bars, Plates, and Shells* (Bull Ridge Publishing, Blacksburg, VA, 2006).
[2] E. Cerda and L. Mahadevan, Geometry and Physics of Wrinkling, Phys. Rev. Lett. **90**, 074302 (2003).
[3] J. Genzer and J. Groenewold, Soft matter with hard skin: From skin wrinkles to templating and material characterization, Soft Matter **2**, 310 (2006).
[4] D.-Y. Khang, J. A. Rogers, and H. H. Lee, Mechanical buckling: Mechanics, metrology, and stretchable electronics, Adv. Funct. Mater. **19**, 1526 (2009).
[5] J. Yin, Z. Cao, C. Li, I. Sheinman, and X. Chen, Stress-driven buckling patterns in spheroidal core/shell structures, Proc. Natl. Acad. Sci. USA **105**, 19132 (2008).
[6] G. Domokos, W. Fraser, and I. Szeberényi, Symmetry-breaking bifurcations of the uplifted elastic strip, Physica D **185**, 67 (2003).
[7] G. Vliegenthart and G. Gompper, Forced crumpling of self-avoiding elastic sheets, Nat. Mater. **5**, 216 (2006).
[8] A. Lobkovsky, S. Gentges, H. Li, D. Morse, and T. A. Witten, Scaling properties of stretching ridges in a crumpled elastic sheet, Science **270**, 1482 (1995).
[9] D. Moldovan and L. Golubovic, Buckling Dynamics of Compressed Thin Sheets (Membranes), Phys. Rev. Lett. **82**, 2884 (1999).
[10] H. Jain, S. Ghosh, and K. C. Sahu, Compression-controlled dynamic buckling in thin soft sheets, Phys. Rev. E **104**, L033001 (2021).
[11] J. Zhang, X. Qiu, C. Wang, and Y. Liu, A general theory and analytical solutions for post-buckling behaviors of thin sheets, J. Appl. Mech. **89**, 061003 (2022).
[12] F. Ebrahimi, M.-S. Shafiee, and M. F. Ahari, Buckling analysis of single and double-layer annular graphene sheets in thermal environment, Eng. Comput. **39**, 625 (2023).
[13] S. P. Timošenko and J. M. Gere, *Theory of Elastic Stability* (McGraw-Hill, New York, 1961).
[14] P. L. Teed, History of Strength of Materials. Stephen P. Timoshenko. McGraw-Hill, 1953. 452 pp. Diagrams and Photographs. 71s. 6d. net., Aeronaut. J. **57**, 826 (1953).
[15] H. Noguchi, Anisotropic surface tension of buckled fluid membranes, Phys. Rev. E **83**, 061919 (2011).
[16] M. Hu, P. Diggins IV, and M. Deserno, Determining the bending modulus of a lipid membrane by simulating buckling, J. Chem. Phys. **138**, 214110 (2013).
[17] J. Stecki, Correlations in simulated model bilayers, J. Chem. Phys. **120**, 3508 (2004).
[18] W. K. den Otter, Area compressibility and buckling of amphiphilic bilayers in molecular dynamics simulations, J. Chem. Phys. **123**, 214906 (2005).
[19] H. Noguchi and G. Gompper, Meshless membrane model based on the moving least-squares method, Phys. Rev. E **73**, 021903 (2006).
[20] J. Eid, H. Razmazma, A. Jraij, A. Ebrahimi, and L. Monticelli, On calculating the bending modulus of lipid bilayer membranes from buckling simulations, J. Phys. Chem. B **124**, 6299 (2020).
[21] J. Eid, H. Greige-Gerges, L. Monticelli, and A. Jraij, Elastic moduli of lipid membranes: Reproducibility of AFM measures, Chem. Phys. Lipids **234**, 105011 (2021).
[22] K. V. Pinigin, Determination of elastic parameters of lipid membranes with molecular dynamics: A review of approaches and theoretical aspects, Membranes **12**, 1149 (2022).
[23] E. Lac, D. Barthes-Biesel, N. Pelekasis, and J. Tsamopoulos, Spherical capsules in three-dimensional unbounded stokes flows: Effect of the membrane constitutive law and onset of buckling, J. Fluid Mech. **516**, 303 (2004).

[24] M. Lenz, D. J. G. Crow, and J.-F. Joanny, Membrane Buckling Induced by Curved Filaments, Phys. Rev. Lett. **103**, 038101 (2009).

[25] R. B. Gennis, *Biomembranes: Molecular Structure and Function* (Springer, New York, 1989).

[26] W. Helfrich, Elastic properties of lipid bilayers: Theory and possible experiments, Z. Naturforsch. C **28**, 693 (1973).

[27] W. Helfrich, The size of bilayer vesicles generated by sonication, Phys. Lett. A **50**, 115 (1974).

[28] E. Evans and W. Rawicz, Entropy-Driven Tension and Bending Elasticity in Condensed-Fluid Membranes, Phys. Rev. Lett. **64**, 2094 (1990).

[29] T. Baumgart, B. R. Capraro, C. Zhu, and S. L. Das, Thermodynamics and mechanics of membrane curvature generation and sensing by proteins and lipids, Annu. Rev. Phys. Chem. **62**, 483 (2011).

[30] F. Jülicher and R. Lipowsky, Domain-induced budding of vesicles, Phys. Rev. Lett. **70**, 2964 (1993).

[31] U. Seifert, Configurations of fluid membranes and vesicles, Adv. Phys. **46**, 13 (1997).

[32] R. Lipowsky, Spontaneous tubulation of membranes and vesicles reveals membrane tension generated by spontaneous curvature, Faraday Discuss. **161**, 305 (2013).

[33] U. Seifert, K. Berndl, and R. Lipowsky, Shape transformations of vesicles: Phase diagram for spontaneous-curvature and bilayer-coupling models, Phys. Rev. A **44**, 1182 (1991).

[34] F. Jülicher and R. Lipowsky, Shape transformations of vesicles with intramembrane domains, Phys. Rev. E **53**, 2670 (1996).

[35] F. Brochard and J. Lennon, Frequency spectrum of the flicker phenomenon in erythrocytes, J. Phys. France **36**, 1035 (1975).

[36] M. Schneider, J. Jenkins, and W. Webb, Thermal fluctuations of large cylindrical phospholipid vesicles, Biophys. J. **45**, 891 (1984).

[37] M. Schneider, J. Jenkins, and W. Webb, Thermal fluctuations of large quasi-spherical bimolecular phospholipid vesicles, J. Phys. France **45**, 1457 (1984).

[38] J. Faucon, M. Mitov, P. Méléard, I. Bivas, and P. Bothorel, Bending elasticity and thermal fluctuations of lipid membranes. theoretical and experimental requirements, J. Phys. France **50**, 2389 (1989).

[39] J. Henriksen, A. C. Rowat, and J. H. Ipsen, Vesicle fluctuation analysis of the effects of sterols on membrane bending rigidity, Eur. Biophys. J. **33**, 732 (2004).

[40] E. Kreyszig, *Differential Geometry* (Courier Corporation, North Chelmsford, MA, 2013).

[41] M. P. Do Carmo, *Differential Geometry of Curves and Surfaces: Revised and Updated Second Edition* (Courier Dover Publications, New York, 2016).

[42] H. Lodish, A. Berk, C. A. Kaiser, C. Kaiser, M. Krieger, M. P. Scott, A. Bretscher, H. Ploegh, P. Matsudaira *et al.*, *Molecular Cell Biology* (Macmillan, New York, 2008).

[43] J. A. McNew, H. Sondermann, T. Lee, M. Stern, and F. Brandizzi, GTP-dependent membrane fusion, Annu. Rev. Cell Dev. Biol. **29**, 529 (2013).

[44] R. Lipowsky, Remodeling of membrane shape and topology by curvature elasticity and membrane tension, Adv. Biol. **6**, 2101020 (2022).

[45] M. Hu, D. H. de Jong, S. J. Marrink, and M. Deserno, Gaussian curvature elasticity determined from global shape transformations and local stress distributions: A comparative study using the Martini model, Faraday Discuss. **161**, 365 (2013).

[46] M. Hu, J. J. Briguglio, and M. Deserno, Determining the Gaussian curvature modulus of lipid membranes in simulations, Biophys. J. **102**, 1403 (2012).

[47] M. Zelisko, F. Ahmadpoor, H. Gao, and P. Sharma, Determining the Gaussian Modulus and Edge Properties of 2D Materials: From Graphene to Lipid Bilayers, Phys. Rev. Lett. **119**, 068002 (2017).

[48] V. Harmandaris and M. Deserno, A novel method for measuring the bending rigidity of model lipid membranes by simulating tethers, J. Chem. Phys. **125**, 204905 (2006).

[49] W. D. den Otter and S. A. Shkulipa, Intermonolayer friction and surface shear viscosity of lipid bilayer membranes, Biophys. J. **93**, 423 (2007).

[50] S. A. Shkulipa, Computer simulations of lipid bilayer dynamics, Ph.D. thesis, University of Twente, 2006, https://ris.utwente.nl/ws/portalfiles/portal/6070110/thesis_Shkulipa.pdf.

[51] E. G. Brandt, A. R. Braun, J. Sachs, J. Nagle, and O. Edholm, Interpretation of fluctuation spectra in lipid bilayer simulations, Biophys. J. **100**, 2104 (2011).

[52] R. Phillips, J. Kondev, J. Theriot, and H. Garcia, *Physical Biology of the Cell* (Garland Science, New York, 2012).

[53] J. Kierzenka and L. F. Shampine, A BVP Solver based on residual control and the Maltab PSE, ACM Trans. Math. Softw. **27**, 299 (2001).